ELSEVIER

Journal of Magnetism and Magnetic Materials 222 (2000) 54–64

journal of magnetism and magnetic materials

www.elsevier.com/locate/jmmm

Preparation of yttrium–iron-garnet nanocrystals dispersed in nanosize-pore glass

Susamu Taketomi*,[1,a], Christopher M. Sorensen[a], Kenneth J. Klabunde[b]

[a]*Department of Physics, Kansas State University, Manhattan, KS 66506, USA*
[b]*Department of Chemistry, Kansas State University, Manhattan, KS 66506, USA*

Received 7 June 2000

Abstract

Amorphous yttrium–iron-garnet (YIG) nanoparticles were dispersed in kerosene solvent and these colloids were introduced into the nanosize pores of controlled pore glass (CPG). After heat treatment, a YIG nanocrystal-dispersed glass was obtained and observed by electron microscopy. The compounds prepared with different pore size CPG under different heat treatment conditions were identified by X-ray diffraction. For samples with a 292-nm-pore-size CPG matrix which were calcined for 2 h, only YIG was observed up to a 800°C calcination temperature. However, at a heat treatment of 2 h at 900°C, the YIG particles decomposed and many kinds of iron and yttrium silicate compounds were formed. In a 16 h treatment at 675°C, yttrium silicate was also prepared besides YIG. On the other hand, only YIG nanocrystals formed when a rapid temperature rise up to 890°C was followed by immediate cooling. It was also found that iron and yttrium silicates decomposed and iron oxide and yttrium oxide formed by high-temperature treatment at 1200°C. A very rare iron oxide ε-Fe_2O_3 was also found in some samples.

PACS: 75.50.Tt; 81.05.Pj; 75.50.Ss; 85.70.Sq

Keywords: Alkoxide method; Magnetic nanoparticle-glass composite; Vycor glass; Thirsty glass; Controlled pore glass; Yttrium–iron-garnet; High-density magnetooptical information storage

1. Introduction

Magnetic fine particles are very attractive objects of magnetic research. This is because they are single magnetic domain particles and accordingly their magnetic properties and their mutual interaction can be studied without magnetic domain effects [1,2]. Moreover, quantum size effects [3] and the magnetic quantum tunneling effects [4–6] can be studied because of their nanoparticle dimension. In addition, from an industrial viewpoint, they are applicable to media for high-density magnetic or magnetooptical information storage. For these reasons many studies on the preparation of many different magnetic nanosize particles by many different methods have been undertaken [7–15]. The magnetic fine particles, however, tend

* Corresponding author. Tel.: +1-785-532-5987; fax: +1-785-532-6806.
E-mail address: staketom@phys.ksu.edu (S. Taketomi).
[1] Permanent address: Matsumoto Yushi-Seiyaku Co. Ltd., Yao, Osaka 581-0075, Japan.

0304-8853/00/$ - see front matter
PII: S0304-8853(00)00533-3

to spontaneous coagulation by mutual magnetic attraction due to their magnetic dipole moment, and their intrinsic magnetic characteristics are often smeared by the coagulation even though very fine magnetic particles were successfully prepared. There have been several methods developed to prevent the coagulation of magnetic fine particles, such as to disperse the magnetic fine particles in an organic binder (magnetic pigment or magnetic tape [16]), or to disperse the particles in a solvent with the aid of surfactant or surface-active agents (magnetic fluids [17]). These methods use mechanical stirring to disperse the particles, and a considerable portion of the particles still remain coagulated if the concentration of the particles is high.

New technologies for dispersion of the magnetic fine particles in glass or polymer matrices were developed to reduce coagulation. The precursors of the magnetic fine particles were dispersed in the sol-state glass precursor, and the magnetic fine particles were precipitated in the solidified glass, or the magnetic fine particles were introduced into the pores in the porous glass [18–24]. The advantages of these methods are as follows.

1. It is possible to heat-treat the precursor of the magnetic fine particles in the glass matrix at higher temperature because glass is more stable than organic binder.
2. It is easy to disperse the precursor particles in the sol precursor of the glass without coagulation because magnetic fine particle precursors are usually nonmagnetic.
3. Glass matrix is a tough complex material without hysteresis and high initial magnetic susceptibility can be obtained.
4. The magnetooptical effect of the magnetic fine particles can be studied because the glass matrix is transparent to visible light.

Up to now, however, the prepared magnetic fine particles were only simple elements such as iron, cobalt or compounds of simple crystal structures e.g. such as iron oxide. Because the precipitation of the ion precursor in the glass matrix, or ion sputtering on the porous glass is used, it is difficult to control the preparation of magnetic fine particles of complex crystal structure.

We have already successfully prepared amorphous yttrium–iron-garnet (YIG) nanoparticles by an alkoxide method [25,26]. (see the next section). In this paper we describe how we introduced these YIG nanoparticles into the pores of porous glass, controlled pore glass (CPG), and heat-treated these compound to obtain nanocrystal YIG particles dispersed in the glass.

2. Experimental

2.1. Preparation method

The amorphous YIG nanoparticles were prepared by the alkoxide method, i.e., iron ethoxide and yttrium butoxide were mixed and hydrolyzed to prepare amorphous YIG nanoparticles of 9 nm mean diameter, expressed by the chemical reaction,

$$5Fe(OEt)_3 + 3Y(OBu)_3 + 12H_2O \rightarrow [Y_3Fe_5O_{12}]\downarrow + 15EtOH + 9BuOH, \quad (1)$$

where Et and Bu denote ethyl and butyl groups, respectively [25]. These particles were dispersed in kerosene solvent with the aid of hydrocarbon surfactant and a stable amorphous YIG colloidal solution was obtained. The method for coating the colloid on an ordinary quartz plate and calcining it were reported earlier [27,28]. After calcination YIG particles transformed to nanocrystalline YIG and made a sponge-like film without particle size growth or fusion [28]. In the present work, instead of coating the colloid on the quartz plate, the colloid was absorbed in the pores of CPG. The CPG that we used in the present study was a powder of porous amorphous silica the mean diameter of each grain was distributed from 37 to 125 μm and their shape is irregular.

The CPG is prepared as follows [29–31]. First a ternary oxide melt (SiO_2–B_2O_3–Na_2O) is rapidly cooled and it solidifies into a homogeneous glass. After reheating and annealing at elevated temperature, it segregates into two interconnected phases. One of them is almost pure silica and the other is sodium borate with some silica dissolved. After removing the sodium borate phase by acid and cleaning silica debris from the pores, CPG is

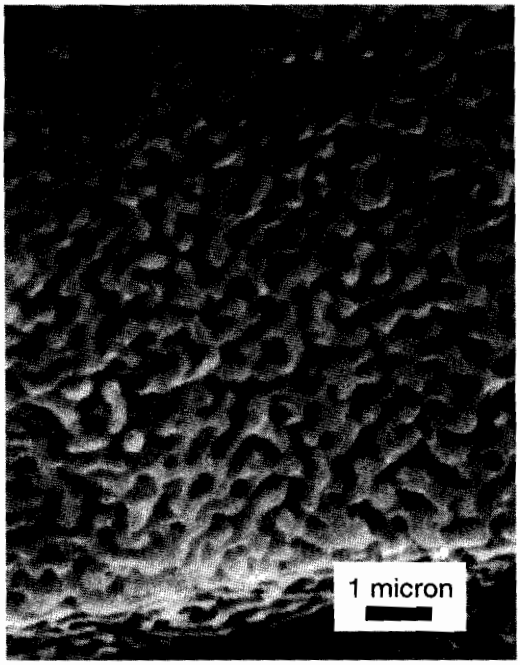

Fig. 1. Carbon replica scanning electron micrograph of CPG surface. By courtesy of CPG Inc. (see footnote 2).

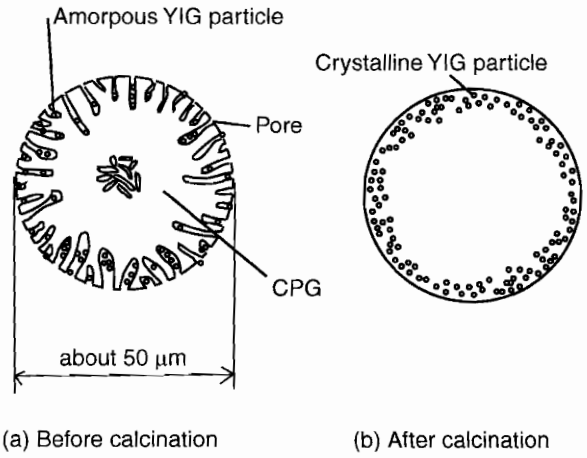

Fig. 2. Schematic figure of CPG with YIG nano particles. Though Fig. 2(a) is a spherical grain showing the pores in the periphery and center areas, the real CPG grains are irregularly shaped and the pores exist in all the region of the grain.

prepared. The CPG contains traces of B_2O_3 and Na_2O which are considered to play a role in the catalysis of the reaction of SiO_2 and YIG particles. Fig. 1 is scanning electron microscope (SEM) photograph of the carbon replica from the CPG surface.[2] Fig. 2 is the schematic figure of a CPG grain. The real grains are irregular and the pores exist in all the region of the grains. The colloidal precursors of YIG nanoparticles were absorbed in the pores of the CPG. After evaporation of the solvent, the amorphous YIG particles were left in the pores (see Fig. 2a). After heat treatment, the pores were fused and at the same time YIG particles were crystallized and embedded in the glass (see Fig. 2b).

In the present study we used four CPGs with different pore size distribution. Their mean pore sizes and size distributions were 48.6 nm (±3.9%) provided by W. Haller of National Institute of Standard and Technology [30], 114 nm (±5.2%), 204 nm (±11.5%), and 292 nm (±7.1%) purchased from CPG Inc. (see footnote 2), respectively. The powder size of the first sample was distributed between 75 and 125 μm while the rests were between 37 and 74 μm. An electric furnace was used for calcination of the samples. The temperature was increased at the rate of 200°C/h from room temperature as high as T_0 and the temperature was held for t_0 h. Then the samples were cooled to room temperature. The characteristics of the samples are tabulated in Table 1. They were calcined in air except samples B_3 and D which were calcined in a N_2 gas environment.

2.2. Characterization methods

2.2.1. Transmission electron microscope sample preparation

The calcined samples were ground with an agate mortar to reduce the grain size from about 50 μm to submicron in dimension to transmit the electron beam. The milling powder was mostly pure silica without YIG particles because the amorphous YIG particles in the original CPG grains were concentrated only in 0.5 μm subsurface layer. Significant color changes were observed after removing this subsurface layer. For example, sample B_4 was

[2] CPG Inc. Catalogue, 3 Borinski Road, Lincoln Park, NJ 07035, USA.

Table 1
Characteristics of samples[a]

Samp.	T_0	t_0	Prepared compounds identified from XRD	D
A_1	700	2	Cristobalite(1), $Fe_5Y_3O_{12}$	4.2
A_2	800	2	Cristobalite(1), $Fe_5Y_3O_{12}$	37
A_3	850	2	Cristobalite(1), $Fe_5Y_3O_{12}$, $Y_2Si_2O_7$(1), Fe_2SiO_4(1), Y_2SiO_5	Unknown
A_4	900	2	Cristobalite(1), α-Fe_2O_3, $Y_2Si_2O_7$(1), $Y_2Si_2O_7$(2), Fe_2SiO_4(2), Y_2SiO_5	None
A_5	1000	2	Cristobalite(1), α-Fe_2O_3, $Y_2Si_2O_7$(1), $Y_2Si_2O_7$(2), Fe_2SiO_4(2), Y_2SiO_5	None
A_6	675	16	Cristobalite(1), $Fe_5Y_3O_{12}$, $Y_2Si_2O_7$(1)	11.2
A_7	700	16	Cristobalite(1), $Fe_5Y_3O_{12}$, Y_2SiO_5(1)	22.0
A_8	793	0.1	Cristobalite(1), $Fe_5Y_3O_{12}$, $Y_2Si_2O_7$(1)	37.0
A_9	890	0	Quartz, $Fe_5Y_3O_{12}$	41.0
B_1	700	2	Cristobalite(2), $Fe_5Y_3O_{12}$, Y_2SiO_5	Unknown
B_2	800	2	Cristobalite(1), ε-Fe_2O_3, Y_2O_3,	None
B_3	900	2	Cristobalite(1), $Y_2Si_2O_7$(1), $Y_2Si_2O_7$(2), Y_2SiO_5, Fe_2SiO_4(1)	None
B_4	1200	2	Cristobalite(2), α-Fe_2O_3, Y_2O_3	None
C	800	2	Cristobalite(1), $Fe_5Y_3O_{12}$	Unknown
D	900	2	Cristobalite(1), ε-Fe_2O_3, $Y_2Si_2O_7$(1), $Y_2Si_2O_7$(2)	None

[a] T_0: calcination temperature (°C), t_0: calcination time (h), D: YIG nanocrystal's mean diameter (nm). sample A_i (i = 1–9): CPG pore size before calcination 292 nm, sample B_i (i = 1–4): CPG pore size before calcination 48.6 nm, sample C: CPG pore size before calcination 204 nm, sample D: CPG pore size before calcination 114 nm. The compounds were identified according to the Powder Data File of Joint Committee on Powder Diffraction Standard (JCPDS). The compounds correspond to the JCPDS number, respectively. Cristobalite(1): 39-1425, cristobalite(2): 76-0936, quartz: 83-2465, $Fe_5Y_3O_{12}$: 43-0507, $Y_2Si_2O_7$(1): 45-0042, $Y_2Si_2O_7$(2): 21-1459, Fe_2SiO_4(1): 71-1667, Fe_2SiO_4(2): 72-0297, Y_2SiO_5: 21-1461, α-Fe_2O_3: 80-2377, ε-Fe_2O_3: 16-0653, Y_2O_3: 44-0399.

tinged with deep red color due to α-Fe_2O_3 which was formed by decomposition of YIG particles during calcination. After grinding, the color changed to white pink because of white cristobalite in the core of CPG grains revealed by grinding. The ground powder was put in a vial filled with 97% ethanol and stirred strongly. Before all the fragments deposited in the bottom of the vial, the supernatant liquid was removed so that excessive pure silica fragments were removed. In fact, the specific gravity of CPG fragments which contained YIG nanocrystals was greater than that of pure CPG fragments. In addition, the former fragments were easy to coagulate due to the YIG magnetic attraction. Accordingly, the CPG fragments with YIG nanocrystals deposited faster than the pure CPG fragments. Taking advantage of this nature, we separated the CPG fragments. This process was done several times. Lastly as soon as the liquid was stirred strongly, a droplet of the liquid was put on polymer film of a copper mesh and the CPG fragments were observed by two transmission electron microscopes (TEM), a Philips 201 and a CM100, operating a 100 kV.

2.2.2. *X-ray diffraction*

Phase composition of the ground samples which were prepared for TEM observation was investigated by X-ray diffraction (XRD) (XDS2000 Scintag Inc.) To increase the signal/background ratio from YIG particles, the slit width of the diffractometer was increased five times and the measuring time was increased 20 times in comparison with the ordinary slit width and the measuring time, respectively. Despite that, the diffraction intensity from YIG particles was very low (Fig. 3 for sample A_8). In Fig. 3, the diffraction intensity increases with angle decrease due to the small angle peak of the polymer substrate. The diffraction peak width widening due to the slit width was compensated by calibration using standard micron size multicrystalline quartz. Using the half value width of diffraction

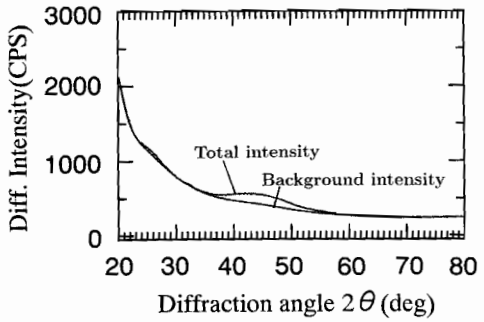

Fig. 3. The total and background X-ray diffraction intensity of sample A_6.

peaks, Δ and Δ_{st} for the YIG nanocrystals of the present samples and the standard quartz sample, respectively, the mean crystalline size, D, of YIG nanoparticles in the silica matrix was determined by

$$D = \frac{0.9\lambda}{(\Delta - \Delta_{st})\cos\theta}, \quad (2)$$

where $\lambda = 1.54$ Å is the X-ray wavelength and 2θ is the diffraction angle.

3. Results and discussion

The fragments which contained YIG particles or reacted YIG particles were observed very rarely.

Fig. 4 is the TEM photograph of sample A_1 calcined for 2 h at 700°C. The characteristics of the samples are tabulated in Table 1. The small black dots in the silica matrix are the crystalline YIG particles as indicated by XRD in the lower part of Fig. 7. Large particles are pure silica fragments. The melting temperature of CPG is between 900 and 1000°C. The region with YIG particles easily melted or softened at less than 700°C presumably because the YIG particles served as contaminants and promoted pore closure of CPG. The selected area electron diffraction (SAED) observation was done on the same sample, but we observed no diffraction patterns. As mentioned later, XRD results of the same sample showed the existence of cristobalite. Accordingly from this SAED result and XRD results it is concluded that a very small portion of the matrix silica was crystallized but that the amount of

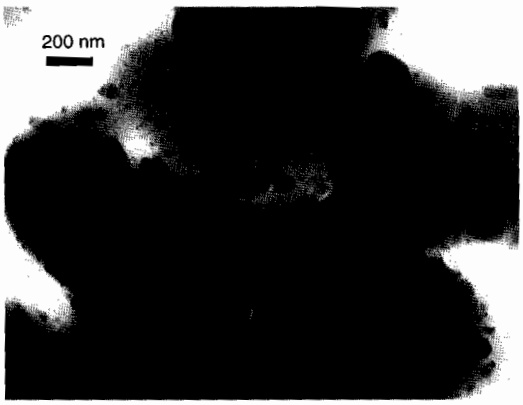

Fig. 4. TEM photograph of sample A_1: $T_0 = 700$°C, $t_0 = 2$ h, the mean pore size of CPG before calcination was 292 nm.

crystallized silica, or cristobalite, was so small that we could not detect the electron diffraction lines of cristobalite in the TEM specimen. A similar speculation was applicable for YIG particles. Refer to the XRD discussion of the same sample in the next paragraph. The diameter of the electron beam which irradiated the sample was 5 μm. Accordingly we could not make individual particle's identification in the present study.

Figs. 5a and b are the bright-field image and SAED pattern of sample A_2. For Fig. 5b, both right and left sides of photographs were printed from the same negative film but with different printing exposure time due to the large difference in brightness of the diffraction patterns. Cristobalite and YIG were identified from the SAED patterns, which is consistent with the result of XRD analysis in Fig. 7.

Fig. 6a is the bright-field image of the fragments of sample A_5. The nanoparticles are dispersed and embedded in the silica matrix. Their identification is discussed in the XRD analysis section. We also found peculiar fragments in this sample. Fig. 6b is the bright-field image of the same sample but at different region. There are peculiar parallel stripes in the silica fragment. They may be the YIG particles' traces that have reacted with the silica matrix. Fig. 6c is the SAED pattern of the same sample. Y_2SiO_5 and Fe_2SiO_4 were identified from this diffraction pattern.

Now let us discuss the XRD results. Fig. 7 shows the XRD patterns from the samples after calcination

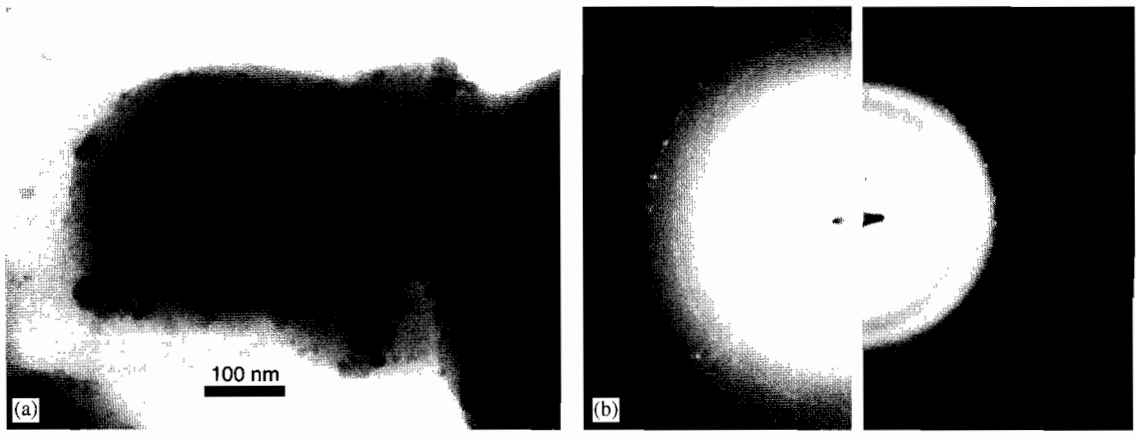

Fig. 5. TEM photograph of sample A_2. $T_0 = 800°C$, $t_0 = 2$ h, the mean pore size of CPG before calcination was 292 nm: (a) bright-field image, (b) selected area electron diffraction pattern. The left- and right-hand-side photographs are printed from the same negative film but with different exposure time.

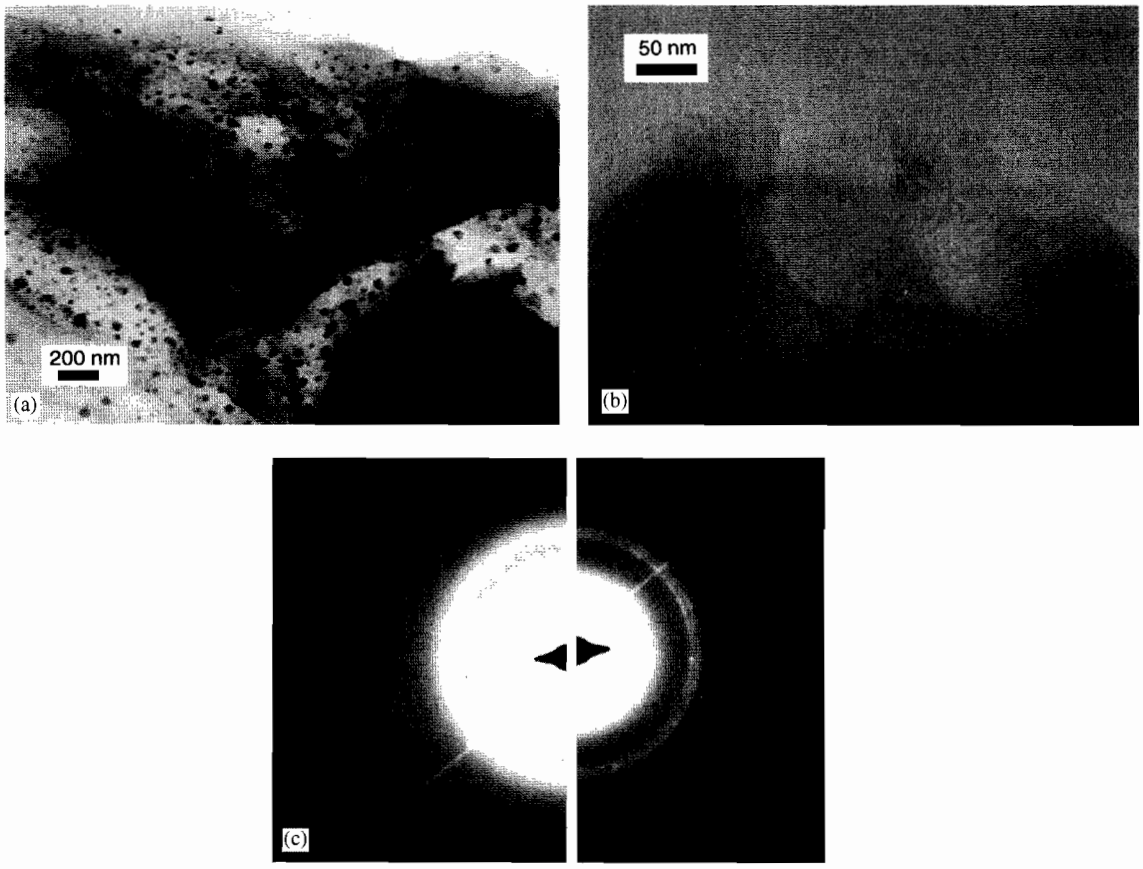

Fig. 6. TEM photograph of sample A_3. $T_0 = 1000°C$, $t_0 = 2$ h, the mean pore size of CPG before calcination was 292 nm: (a) and (b) bright field image of different points, (c) selected area electron diffraction pattern. The left- and right-hand-side photographs are printed from the same negative film but with different exposure time.

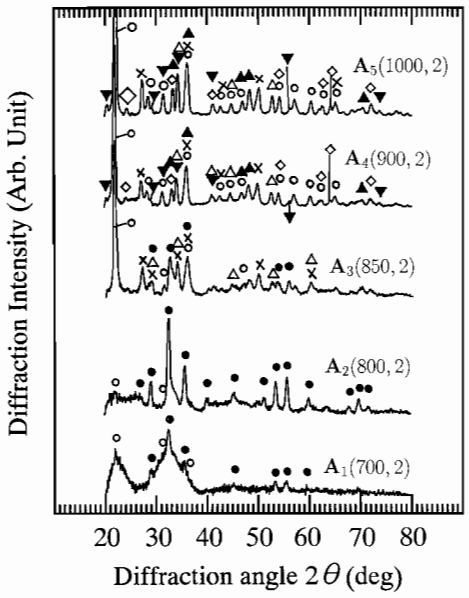

Fig. 7. Calcination temperature, T_0, dependence of XRD patterns for samples of large pore CPG. The calcination time, $t_0 = 2$ h, for all samples, the pore size of CPG before calcination was 292 nm for all samples. The figures in parentheses are the calcination temperature (°C) and time (h), respectively. Peak marks are as follows and they are used in common in Figs. 8–10. ●: $Fe_5Y_3O_{12}$, ○: cristobalite(1), ⊙: cristobalite(2), ⊗: quartz, △: $Y_2Si_2O_7$(1), ▲: $Y_2Si_2O_7$(2), ▽: Fe_2SiO_4(1), ▼: Fe_2SiO_4(2), ×: Y_2SiO_5, ◇: α-Fe_2O_3, ◆: ε-Fe_2O_3, □: Y_2O_3.

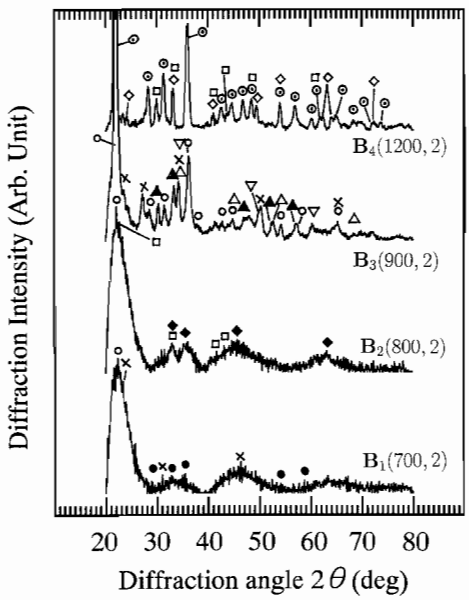

Fig. 8. Calcination temperature, T_0, dependence of XRD patterns for samples of small pore CPG. The calcination time, $t_0 = 2$ h, for all samples, the pore size of CPG was 48.6 nm for all samples. The figures in parentheses are the calcination temperature (°C) and time (h), respectively. Peak marks are listed in the caption of Fig. 7.

at the temperatures from 700°C to 1000°C (samples A_1–A_5). The pore size of CPG before calcination was 292 nm and the calcination time, t_0, was 2 h for all the samples. The XRD curves in this paper are all shown without smoothing treatment. The peak marks, ○, ●, ⊙, …, denote individual compounds which are shown in Fig. 7. These marks are common in Figs. 8–10.

A YIG crystal was prepared for the sample of the calcination temperature, $T_0 = 700$°C. The mean crystalline size, D, of the YIG nanoparticles was estimated by the half value width, Δ, of the (4 2 0) peak ($2\theta = 32.314°$) and Δ_{st} of the (1 1 2) peak ($2\theta = 50.138°$) of standard multicrystalline quartz, using expression (2). The D value for each sample is shown in Table 1. YIG's D increases rapidly with the calcination temperature.

Many iron silicate and yttrium silicate compounds were prepared by the reaction of YIG particles and CPG or silicate for the samples of T_0 above 850°C. The identified products are tabulated in Table 1. In addition, there are a few peaks which cannot be identified. There are several polymorphisms for the same chemical formula of iron silicate and yttrium silicate. Therefore, it may be that several kinds of polymorphism of iron silicate and yttrium silicate were prepared in the contact region between YIG particles and CPG.

Fig. 8 shows the XRD patterns of the samples of T_0 at 700°C and up to 1200°C with small CPG pores (samples B_1–B_4). The calcination time, t_0 was 2 h and the mean pore diameter before calcination was 48.6 nm for all the samples. All the samples were calcined in the air except sample B_3 which was calcined in a N_2 gas environment. The YIG particles were decomposed to different compounds for the samples of $T_0 \geqslant 800$°C. In addition, the iron and yttrium silicate disappeared and YIG particles decomposed almost to α-Fe_2O_3 and Y_2O_3 for the sample of $T_0 = 1200$°C.

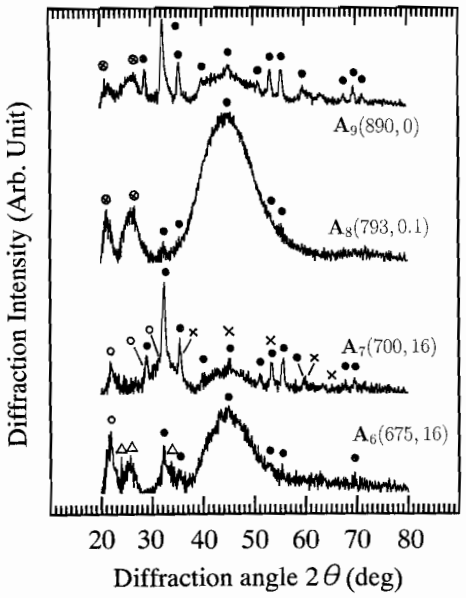

Fig. 9. Calcination time, t_0, dependence of XRD patterns. The pore size of CPG was 292 nm for all samples. The figures in parentheses are the calcination temperature (°C) and time (h), respectively. Peak marks are listed in the caption of Fig. 7.

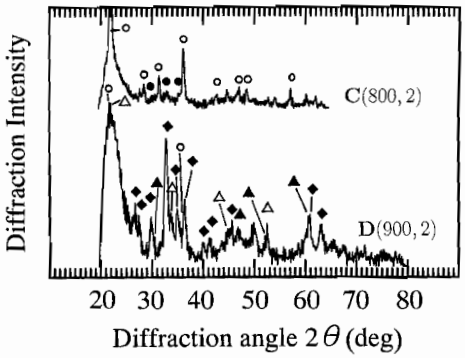

Fig. 10. XRD patterns of samples with CPG pores, 114 and 204 nm. The figures in parentheses are the calcination temperature (°C) and time (h), respectively. Peak marks are listed in the caption of Fig. 7.

Fig. 9 shows XRD patterns of the samples for different calcination time, t_0 from 0 to 16 h (samples A_6–A_9) T_0 was not the same for these samples. The meaning of $T_0 = 890$, $t_0 = 0$ for sample A_9 is as follows. The furnace temperature was increased as high as 890°C at the rate of 200°C/h. The moment the temperature reached $T_0 = 890$°C, the power of the furnace was turned off and the sample temperature was decreased spontaneously. From the result of sample A_6, it was revealed that YIG particles and silicate reacted to form iron and yttrium silicate during long-time heat treatment even at a low-temperature calcination of 675°C. This fact indicates that iron or yttrium silicates are more stable than the separated state of YIG and silica. The formation of the iron and yttrium silicate at such a low temperature may also indicate that the contaminants, B_2O_3 and Na_2O in CPG played a role as catalysts for the reaction of YIG particles and CPG to form yttrium and iron silicate.

Fig. 10 shows the XRD results for the samples of pore size 204 and 114 nm before calcination (samples C and D). Sample D was calcined in a N_2 gas environment. We found ε-Fe_2O_3 prepared in samples B_2 and D. We have already reported that very small amount of ε-Fe_2O_3 was prepared in amorphous YIG nanoparticles [26] ε-Fe_2O_3 is very special iron oxide and only two papers reported the preparation of this material to the best of our knowledge [32,33]. The common features among those papers and ours are that nanoparticles precursor which contained iron ion reacted under the existence of numerous hydroxyl groups. In fact, the present amorphous YIG particles were prepared by hydrolysis and a considerable numbers of the particles had a chemical formula, $(5Fe(OH)_3)(3Y(OH)_3) = Fe_5Y_3O_{12} \cdot 12H_2O$ [25].

From the above experimental results the following speculations are possible. Three different processes occurred in parallel in the present calcination. Fig. 11 contains schematic figures to explain these processes. Fig. 11a is the state before the calcination. Both the particles and the CPG were in an amorphous phase. The radius of the circles which denote oxygen, iron, yttrium and silicon ions, respectively, are proportional to each ion's radius. The first process is the phase transition of YIG particles from amorphous to crystalline state. The second process is the phase transition of CPG from amorphous to cristobalite crystal. These two processes were shown in Fig. 11b. The third process is the reaction of YIG particles and the contacting CPG to prepare iron silicate and yttrium silicate, which is schematically

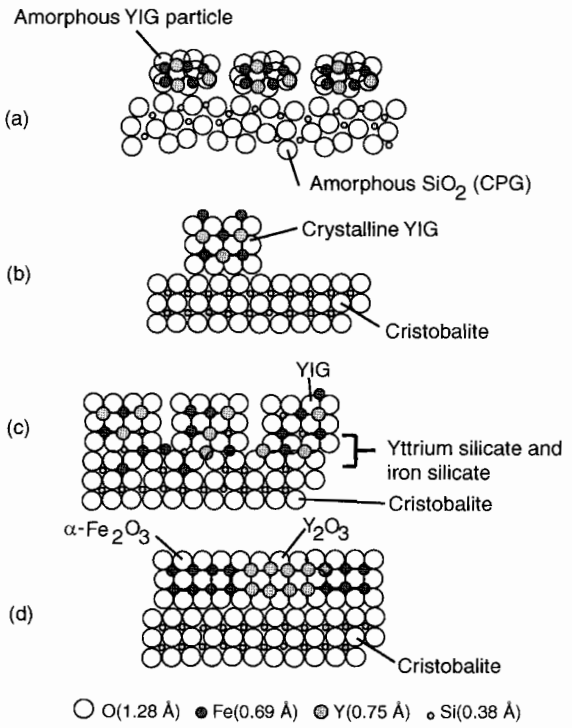

Fig. 11. Schematic figure of heat treatment process of YIG amorphous particles and CPG: (a) Before calcination. Both YIG particles and CPG are amorphous. (b) The crystallization of amorphous YIG particles and amorphous silcate, or CPG. (c) Reaction between YIG particles and CPG on the boundary. (d) Decomposition of iron and yttrium silicate to α-Fe_2O_3 and Y_2O_3 at high temperature calcination. The circles' radius is proportional to each ion radius.

shown in Fig. 11c. The third process proceeds slowly compared with the first and second processes in the low-temperature calcination. Accordingly, it seems that only the first and second processes proceed in the low-temperature calcination for short calcination time. The CPG of small pores has large surface area contacting the YIG particles, and accordingly the third process proceeds notably even in low temperature short time calcination. In addition, in the calcination of high temperature as high as 1200°C, the yttrium and iron silicate transformed to more stable compounds, α-Fe_2O_3, Y_2O_3, and SiO_2 (see Fig. 11d).

In conclusion, for the purpose of preparing YIG nanocrystals dispersed in silica glass, the calcination should be carried out by increasing the temperature as rapidly as possible and immediately after the temperature reaches a temperature near 900°C, at which the amorphous YIG particles are crystallized, the temperature should be decreased lest the reaction between YIG and silica should occur. In a forthcoming paper, we will discuss the magnetic and magnetooptical properties of these samples.

4. Conclusion

Amorphous yttrium iron garnet (YIG) nanoparticles were prepared by an alkoxide method, and they were dispersed in kerosene solvent with the aid of surfactants. The YIG colloids were introduced into the nanosize pores of a special glass, controlled pore glass (CPG), by absorbing the colloidal solution. After evaporation of the solvent, the amorphous YIG particles in the pores were crystallized by heat treatment and YIG nanocrystal-dispersed glass was obtained. We studied how these YIG particles were dispersed in the glass by electron microscopy. Using different CPG materials of the pore size 48.6, 114, 204, and 292 nm, respectively and with different heat treatment condition, we prepared many different samples and identified their prepared compounds by X-ray diffraction. It was revealed that the presence of the YIG particles in the pores promoted pore fusion and YIG particles were imbedded in the glass even at calcination temperature as low as 700°C. It was also revealed that in some heat treatment conditions, many kinds of iron silicates and yttrium silicates were prepared by reaction of YIG particles and CPG, or silica. For the experiments of the samples with 292 nm pore size CPG before calcination, the following results were obtained. In 2 h short calcination interval experiment, the amorphous YIG particles and CPG, or the amorphous silica transformed to the crystalline YIG and cristobalite, respectively, at the calcination temperature up to 800°C. Additional iron silicate was also prepared from the same raw material at calcination temperature of 850°C. The YIG particles decomposed and many kinds of iron and yttrium silicate compounds were prepared at the calcination temperature as low as 900°C. For the experiments of the samples with 48.6 nm pore size CPG before calcination, the following results were obtained. Additional yttrium

silicate compound was prepared besides YIG even at the calcination temperature as low as 700°C. In a long calcination interval experiment, the yttrium silicate was prepared besides YIG for the calcination condition of temperature of 675°C and 16 h interval with 292 nm pore CPG before calcination. On the contrary if we heat treated the same raw material by raising the temperature rapidly as high as 890°C and immediately cooled it down rapidly, no iron or yttrium silicate was formed but only YIG particles were prepared. From these experimental results, the following speculation is possible. Three different processes proceed by this heat treatment. The first one is the crystallization of amorphous YIG particles. The second one is the crystallization of CPG or the amorphous silica. The third one is the reaction between the YIG particles and CPG to prepare many different kinds of iron and yttrium silicates. The third one is hard to react compared to the former two processes, and it is only recognized in relatively high temperature treatment or long term heat treatment. It was also revealed that iron and yttrium silicates decomposed and iron oxide and yttrium oxide were prepared in high temperature treatment as low as 1200°C. Very rare iron oxide, ε-Fe_2O_3, was also found in some samples.

In conclusion, if we want to prepare the glass dispersed with nanocrystalline YIG particles imbedded in the glass, the following heat treatment is preferable. The temperature of the raw material should be raised quickly to nearly 900°C, and then immediately cooled lest a third process should occur.

Acknowledgements

It is our pleasure to express our sincere thanks to Prof. W. Haller for providing us with part of the CPG used in this work and useful discussions. We also thank Dr. X. M. Lin, Dr. A. Paulsen and Dr. D. Boyle for their help and advise for TEM observations, and CPG Inc. for providing us with a CPG electron micrograph (Fig. 1). We also acknowledge the Kansas State University Biology Microscopy and Image Processing Facility, which has been supported in part by the Kansas NSF EPSCoR Program, by the Kansas NASA EPSCoR Program, by University resources, and by the Kansas Agricultural Experiment Station.

References

[1] S. Taketomi, Phys. Rev. E 57 (1998) 3073.
[2] S. Taketomi, Phys. Rev. E 58 (1998) 1175.
[3] S. Taketomi, H. Takahashi, N. Inaba, H. Miyajima, J. Phys. Soc. Japan 60 (1991) 3426.
[4] J. Tejada, X.X. Zhang, E.M. Chudnovsky, Phys. Rev. B 47 (1993) 14977.
[5] X.X. Zhang, R. Ziolo, E.C. Kroll, X. Bohigas, J. Tejada, J. Magn. Magn. Mater. 140–144 (1995) 1853.
[6] W. Wernsdorfer, E.B. Orozco, K. Hasselbach, A. Benoit, D. Mailly, O. Kubo, H. Nakano, B. Barbara, Phys. Rev. Lett. 79 (1997) 4014.
[7] S. Nafis, G.C. Hajipanayis, C.M. Sorensen, K.J. Klabunde, J. Appl. Phys. 67 (1990) 4478.
[8] Yiping, G.C. Hajipanayis, C.M. Sorensen, K.J. Klabunde, J. Appl. Phys. 67 (1990) 4502.
[9] H.K. Xu, C.M. Sorensen, K.J. Klabunde, G.C. Hajipanayis, J. Mater. Res. 7 (1992) 712.
[10] K.J. Klabunde, Free Atoms, Clusters, and Nanoscale Particles, Academic, San Diego, 1994.
[11] D. Zhang, G. Glavee, K.J. Klabunde, C.M. Sorensen, High Temp. Mater. Sci. 36 (1996) 93.
[12] D. Zhang, K.J. Klabunde, C.M. Sorensen, G.C. Hajipanayis, High Temp. Mater. Sci. 36 (1996) 135.
[13] R.J. Bandaranayake, J.Y. Lin, H.X. Jiang, C.M. Sorensen, J. Magn. Magn. Mater. 169 (1997) 289.
[14] X.M. Lin, C.M. Sorensen, K.J. Klabunde, G.C. Hajipanayis, Langmuir 14 (1998) 7140.
[15] X.M. Lin, C.M. Sorensen, K.J. Klabunde, G.C. Hajipanayis, J. Mater. Res. 14 (1999) 1542.
[16] K. O'Grady, R.G. Gilson, P.C. Hobby, J. Magn. Magn. Mater. 95 (1991) 341.
[17] R.E. Rosensweig, Ferrohydrodynamics, Cambridge University Press, Cambridge, 1985.
[18] R.D. Shull, J.J. Ritter, A.J. Shapiro, L.J. Swartzendruber, L.H. Bennett, J. Appl. Phys. 67 (1990) 4490.
[19] J.K. Vassiliou, V. Mehrotra, M.W. Russell, E.P. Giannelis, R.D. McMichael, R.D. Shull, R.F. Ziolo, J. Appl. Phys. 73 (1993) 5109.
[20] D. Sunil, J. Sokolov, M.H. Rafailovich, B. Kotyuzhanskii, H.D. Gafney, J. Appl. Phys. 74 (1993) 3768.
[21] C. Tsang, H.D. Gafney, D. Sunil, M. Rafailovich, J. Sokolov, R.J. Gambino, J. Appl. Phys. 79 (1996) 6025.
[22] C. Estournes, T. Lutz, J. Happich, T. Quaranta, P. Wissler, J.L. Guille, J. Magn. Magn. Mater. 173 (1997) 83.
[23] A. Mekki, Kh.A. Ziq, J. Magn. Magn. Mater. 189 (1998) 207.
[24] A. Hartridge, A.K. Bhattacharya, C.K. Majumdar, D. Das, S.N. Chintalapudi, J. Magn. Magn. Mater. 183 (1998) L1.

[25] S. Taketomi, K. Kawasaki, Y. Ozaki, S. Yuasa, Y. Otani, H. Miyajima, J. Am. Ceram. Soc. 77 (1994) 1787.
[26] S. Taketomi, Z.R. Dai, F.S. Ohuchi, J. Magn. Magn. Mater. 217 (2000) 5.
[27] S. Taketomi, K. Kawaguchi, Y. Otani, H. Miyajima, K. Kawasaki, Y. Ozaki, IEEE Trans. Magn. 30 (1994) 945.
[28] S. Taketomi, H. Yokoyama, H. Miyajima, J. Appl. Phys. 86 (1999) 5520.
[29] W. Haller, J. Chem. Phys. 42 (1965) 686.
[30] W. Haller, Nature 206 (1965) 693.
[31] W. Haller, Solid Phase Biochemistry, in: W. H. Scouten (Ed.), Wiley, New York, 1983 (Chapter 11).
[32] L. Walter-Levy, M.E. Quemeneur, Compt. Rend. 257 (1963) 3410.
[33] Von R. Schrader, G. Büttner, Z. anorganische algemeine Chem. 320 (1963) 220.